IEEE Access
Multidisciplinary ⋮ Rapid Review ⋮ Open Access Journal

Received 2 August 2024, accepted 1 September 2024, date of publication 4 September 2024, date of current version 16 September 2024.

Digital Object Identifier 10.1109/ACCESS.2024.3454362

RESEARCH ARTICLE

Robust Control for a Battery Charger Using a Quadratic Buck Converter

OSWALDO LÓPEZ-SANTOS[1], (Senior Member, IEEE), CARLOS ANDRÉS TORRES-PINZÓN[2], FREDDY FLORES-BAHAMONDE[3], (Senior Member, IEEE), REHAM HAROUN[1], (Member, IEEE), JUAN ANTONIO GARRIGA[4], (Member, IEEE), HUGO VALDERRAMA-BLAVI[1], (Member, IEEE), AND LUIS MARTÍNEZ-SALAMERO[1], (Life Senior Member, IEEE)

[1]Group of Automatic Control and Industrial Electronics, Universitat Rovira i Virgili (URV), 43007 Tarragona, Spain
[2]Modelling-Electronics and Monitoring (MEM) Research Group, Faculty of Electronic Engineering, Universidad Santo Tomás, Bogotá 110311, Colombia
[3]Energy Transformation Center, Engineering Faculty, Universidad Andrés Bello, Providencia, Santiago 7500735, Chile
[4]Department of Industrial and Building Engineering, University of Lleida, 25003 Lleida, Spain

Corresponding authors: Oswaldo López-Santos (oswaldo.lopez@urv.cat), Carlos Andrés Torres-Pinzón (carlostorresp@usta.edu.co), and Freddy Flores-Bahamonde (freddy.flores@unab.cl)

This work was supported in part by Universidad Santo Tomás, Colombia, under Contract 2024-AI026; in part by Spanish Ministerio de Ciencia, Innovación y Universidades (MICIU) through grant PID2019-111443RB-I00, in part through the grant MSCA IF EF-ST 2020/PCI2021-122066-2B financed by MICIU/AEI/10.13039/501100011033 and by the European Union NextGeneration EU/PRTR; in part through the project PID2023-150839OB-I00 financed by MICIU/AEI/10.13039/501100011033 and FEDER, UE; in part by the Agencia Nacional de Investigación y Desarrollo (ANID) through projects FONDECYT Iniciación 11220863; and in part by the Solar Energy Research Center (SERC) Chile (CONICYT/FONDAP/1523A0006).

ABSTRACT In this paper, the quadratic buck converter (QBC) is proposed as competitive alternative to implement a battery charger. Since QBC is a high order system, the required control is designed to follow the conventional constant-current constant-voltage protocol by means of three loops. Namely, 1) an inner-loop operating in sliding mode to control the current of the closest inductor to the input port providing the proper stability of the system, 2) a first outer loop designed to regulate the battery voltage providing the reference of the inner loop, and finally 3) a second outer loop to regulate the battery current modifying the reference of the voltage loop. Proportional Integral (PI) controllers are used in both outer loops, one of them synthesized by means of the robust loop shaping M-constrained integral gain optimization (RLS-MIGO) method, and the other designed using classical considerations for cascaded controllers. Both simulation and experimental results are presented validating the theoretical study and confirming the feasibility of the proposed control by means of analogue electronics.

INDEX TERMS Battery charger, quadratic buck converter, robust loop shaping, sliding-mode control.

I. INTRODUCTION

Battery energy storage technology has been incorporated during many years in stand-alone photovoltaic applications, uninterruptible power supplies and low-power portable devices. However, nowadays, in additional to traditional applications, that technology plays a key role boosting the modern smart and sustainable electrical systems [1], [2]. The adoption of these systems follows to main patterns. The first on is related to dynamic exchanging of energy involving applications such as utility-scale batteries, behind-the-meter energy storage and micro-grids, while the second one corresponds to rechargeable systems operating without connection to a main source and having certain temporary energy autonomy such as cell phones, drones and electric vehicles (EVs). Considering the amount of power demanded by the latter applications, the advances in battery energy storage are crucial for the electrification of the transportation sector [3], [4], [5], [6]. For EVs, for instance, the batteries can be recharged using battery chargers that are either in-home installed or portable by users, or can be available in charging stations as a part of an electric energy distributed

The associate editor coordinating the review of this manuscript and approving it for publication was Yuh-Shyan Hwang.

infrastructure [7], [8]. The main function of these chargers is to provide the necessary energy to recover the state of charge of the batteries while maintaining their good performance to increase their lifetime. The voltage and power levels of the chargers depend on the application and are defined by the size of the battery array and the expected charging time. For example, battery chargers for electric vehicles can provide between 200 and 1000 V with an output power of up to 350 kW. Depending on the relation between the battery capacity and the transferred power, the charging time varies from minutes to several hours [6], [9]. The advances in semiconductors have increased the maximum output power of the chargers allowing charging times for an EV in less than fifteen minutes. The associated power electronics technology enables the so called fast-charging and ultrafast-charging, which are related with the use of lithium based batteries [10], [11], [12].

The energy processed by a battery charger is transferred from a primary power source to the battery following a charging method. Most of the methods perform the charge in a sequence of stages in which the charger applies a constant DC current or a constant DC voltage. The classical method consist in applying a constant current to the battery until it reaches a predefined voltage level (constant current phase) and then apply that voltage until the battery is completely charged (constant voltage phase). This method is well known as the constant current – constant voltage (CC-CV) protocol [13]. Other methods can use multiple phases of constant current with an increasing reference using steps like in the case of [14] and [15]. The sequence of phases is usually carried out by switching between the controllers related to each phase, which can produce an undesired transient behavior. For that reason, it makes sense to explore a mechanism of soft transition in the CC-CV protocol when commuting the action of the current controller in CC phase to the voltage controller in the CV phase.

Battery chargers can be classified in isolated or non-isolated and can be powered by alternating current (AC chargers) or direct current (DC chargers). The AC chargers are normally composed of two power conversion stages, one performing rectification ensuring a unitary power factor and the other performing regulation of the DC output voltage and current. Instead, the DC chargers can be implemented using a single stage of DC-DC conversion which is fed by a primary system providing a regulated DC output [5], [6]. The selection of the adequate DC-DC power converter in both cases (output stage) depends on the constraints of the application mainly related with the input and output voltage ranges, the rated power and the requirement of galvanic isolation [16]. Among the well-known candidates, we can cite the LLC resonant converter, the phase-shifted full-bridge converter, the interleaved buck converter and the dual active bridge (DAB).

The quadratic buck converter (QBC) has been introduced by D. Maksimovic and S. Cuk [17] and subsequently studied by the research group of E. Carbajal-Gutiérrez et al. exploring modelling and feasible control techniques based on pulse width modulation (PWM) and resistive type load [18], [19], [20]. More recently, the QBC has been studied operating at variable switching frequency with a controller based on sliding mode which has the ability to face constant power loads CPLs [21]. This is a fourth order converter with a single controlled switch that allows a higher reduction in the voltage gain and therefore an increase in the current gain in comparison with the classical buck converter without the need of transformers. The QBC may be a suitable candidate in applications where: a) the DC input voltage is various times higher than the battery array voltage; b) galvanic isolation is not mandatory because it is provided by a previous conversion stage; and c) the required output current is high. An alternative based on the cascade connection of two buck converters is also feasible at the expense of adding complexity; i.e., two controlled switches and the corresponding drivers, but without guarantee of a higher efficiency [22].

Sliding Mode Control (SMC) has been used to control power converters proving to be a superior alternative in terms of simplicity of implementation, speed of response and robustness with respect to linear controllers [23], [24], [25]. All these aspects are more significant in the regulation of a high-order system, such as the QBC. Once the dynamic behavior of the QBC is explored using SMC with the respective switching surface, the global control can be applied using nested loops (multi-loop control) in which an inner loop ensures operation in a sliding mode while an outer loop impose regulation or tracking in a variable of interest [26], [27], [28]. Depending of the requirements of a particular application, the control can involve more than one inner loop and more than one outer loop like the system studied in [29]. A key aspect in the multi-loop implementation is the choice of the variables involved in the sliding surface of the inner loop since the stability depends on it. As it can be verified in [30], [31], and [32], despite the complexity of the power converter, the use of a single inductor current in the sliding surface is a simple and effective choice. An exception is the QBC itself as demonstrated in [21], where the use of the current of an inductor in the sliding surface does not allow a direct stabilization of the converter with a constant power load, but facilitates the subsequent stabilization by an outer loop. Conventionally, the outer loop of the control system is configured using a proportional-integral (PI) controller which offers the solution with the best cost-benefit trade-off.

By definition, robust control is a theoretical approach in which the controller is designed to deal with uncertainty and disturbances. Among the known robust control techniques are the following: H-infinity, quantitative feedback theory (QFT), passivity-based control, Lyapunov-based control and the above-mentioned sliding mode control. One interesting approach developed by K. J. Astrom and H. Panagopoulos is the robust loop shaping M-constrained integral gain optimization method (RLS-MIGO) which has been introduced in the literature at the end of the 1990s [33], [34], [35].

Considering a PI compensator, the method is based in a geometric development that uses both the Nyquist diagram and the space formed by the controller parameters which is a plane in the case of a conventional PI controller. Despite the favorable features of this technique, its application in the power electronics field has taken more than ten years and has been done in a multi-loop system regulating the output voltage of the quadratic boost converter [30]. Shortly after, the same method has been also applied in the control of a pulse width modulated (PWM) inverter [36], and similar approaches using loop-shaping have been implemented in a buck converter [37] and in an islanded microgrid [38]. In the context of battery charging, it makes sense to consider this robust technique because of the intrinsic uncertainty of the battery parameters since they change during the device lifetime and also during the charging process.

This paper proposes a multi-loop control method based on sliding mode to control the QBC as a battery charger. The proposal involves an inner loop of sliding mode control and two nested outer regulation loops to perform the above mentioned CC-CV charging protocol. The sliding surface of the inner loop involves only the inductor current closest to the input port of the converter. The first outer loop implemented using a PI controller regulates the output voltage at a reference value which is fixed for the CV phase. During the CC phase, the outermost loop, which is also implemented using a PI controller, modifies the voltage reference in order to impose the charging current limitation. The nonlinear nature of the QBC loaded by a battery implies that the dynamic behavior changes depending on the operation point and introduces uncertainty in its parameters. For that reason, it makes sense, despite the inherent robustness of the sliding mode control implemented in the inner loop, to ensure the robustness also in the outer loops to cope with the uncertainty of the change and improve the performance of the system. In this paper, this aspect has been taken into account and the PI of the voltage regulation loop is synthesized by applying the RLS-MIGO method. Considering that the closed loop of voltage regulation is robust and the contribution of the outermost controller modifies the reference very slowly, the synthesis of the current controller is performed by using the root locus method and considering the basic fundamentals for the design of cascaded controllers.

The main contributions of this paper are:

1) A complete theoretical analysis of the proposed multi-loop control based on a SMC approach, ensuring robustness and an easy implementation in a high-order system.
2) the application of the proposed multi-loop controller ensuring the charging of a battery system for electromobility applications, extending the work reported in [32].
3) the application of a robust control method to synthesize the PI controller of the voltage regulation loop ensuring the proper operation despite uncertainties in the parameters or the inherent evolution of the operation conditions.
4) the complete description of the numerical methods employed for the synthesis of the controllers and the experimental validation, extending the work presented in [39].

The rest of the paper is organized as follows: Section II presents the circuit analysis used to derive the model of the quadratic buck converter. Section III introduces the theoretical analysis of the inner current control loop developed using sliding mode control. Section IV covers the battery charging system and develops the synthesis of the outer loops to impose the desired CC-CV battery charging protocol. Section V describes the numerical evaluation of the applied methods to design the controllers and the simulation results. Finally, experimental results are presented in Section VI and conclusions are summarized in Section VII.

II. SWITCHED-MODEL OF THE QBC

The electrical circuit of the QBC proposed for battery charging is shown in Figure 1. As it can be noted, the circuit is composed by the inductors L_1 and L_2, the capacitors C_1 and C_2, the diodes D_1, D_2 and D_3, and the controlled switch S_1 which is governed by the control signal $u(t)$. As stated, this circuit provides a wider conversion ratio than the conventional buck converter, since the dc gain between the output voltage and the input voltage is a quadratic function, described by

$$\frac{V_{C_2}}{V_g} = D^2 \tag{1}$$

where V_{C_2} and V_g are the average values of the output and input voltage, and D is the duty cycle of the converter which is defined as the average value of the control signal $u(t)$. As can be observed, the converter is also connected to a battery modeled as the controlled voltage source v_{bat} connected in series with the resistance R_{bat}. Although the resistance R_{bat} slightly varies during the charging process, in the subsequent analysis it is considered constant. The QBC has only one active switch to perform the voltage conversion and its operation is equivalent to have two cascaded buck converters sharing the same control signal. Thus, through the control signal $u(t) = \{0, 1\}$ two configurations are obtained for operation in continuous conduction mode (CCM). Figure 2a shows the ON−state configuration associated to $u(t) = 1$, and Figure 2b the OFF−state configuration, corresponding to $u(t) = 0$. The state vector of the converter is given in (2). In CCM, the dynamics of the QBC can be modelled by means of the bilinear system equation (3).

$$x(t) = \begin{bmatrix} i_{L_1}(t) & v_{C_1}(t) & i_{L_2}(t) & v_{C_2}(t) \end{bmatrix}^T \tag{2}$$

$$\frac{di_{L_1}}{dt} = -\frac{v_{C_1}}{L_1} + \frac{v_g}{L_1}u$$

$$\frac{dv_{C_1}}{dt} = \frac{i_{L_1}}{C_1} - \frac{i_{L_2}}{C_1}u$$

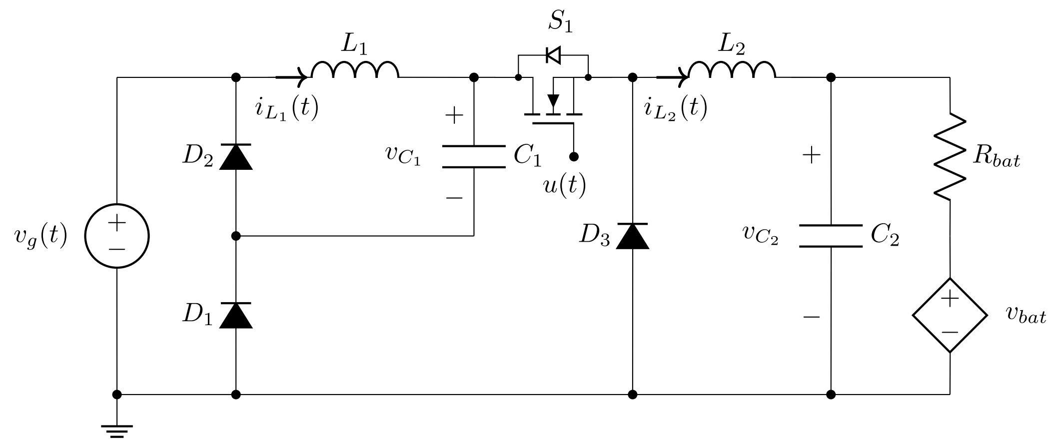

FIGURE 1. **Schematic circuit diagram of a quadratic buck converter feeding a battery type load.**

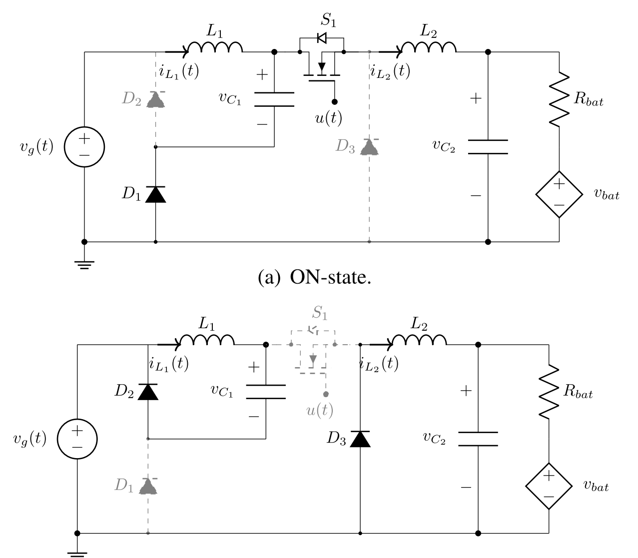

(a) ON-state.

(b) OFF-state.

FIGURE 2. **Quadratic buck circuit configurations.**

$$\frac{di_{L_2}}{dt} = \frac{v_{C_1}}{L_2}u - \frac{v_{C_2}}{L_2}$$
$$\frac{dv_{C_2}}{dt} = \frac{i_{L_2}}{C_2} - \frac{\left(v_{C_2} - v_{bat}\right)}{R_{bat}C_2} \tag{3}$$

III. SLIDING-MODE CONTROL

The switching surface considered in this application is defined as $S(x) = i_{L_1} - k(t)$, where $k(t)$ is provided by an outer control loop. Introducing the invariance conditions $S(\mathbf{x}) = 0$ and $\frac{dS(\mathbf{x})}{dt} = 0$ in (4) results in the equivalent control $u_{eq}(\mathbf{x})$ bounded as follows:

$$0 < \left[u_{eq}(\mathbf{x}) = \frac{L_1\frac{dk}{dt} + v_{C_1}}{V_g}\right] < 1 \tag{4}$$

Now, substituting u by $u_{eq}(\mathbf{x})$ in (3) results in the following ideal sliding dynamics:

$$\frac{dv_{C_1}}{dt} = \frac{k}{C_1} - \frac{L_1}{C_1}\frac{i_{L_2}}{v_g}\frac{dk}{dt} - \frac{i_{L_2}}{C_1}\frac{v_{C_1}}{v_g} = g_1(\mathbf{x})$$
$$\frac{di_{L_2}}{dt} = \frac{L_1}{L_2}\frac{v_{C_1}}{v_g}\frac{dk}{dt} + \frac{v_{C_1}^2}{L_2v_g} - \frac{v_{C_2}}{L_2} = g_2(\mathbf{x})$$
$$\frac{dv_{C_2}}{dt} = \frac{i_{L_2}}{C_2} - \frac{\left(v_{C_2} - v_{bat}\right)}{R_{bat}C_2} = g_3(\mathbf{x}) \tag{5}$$

The coordinates of the equilibrium point are given by:

$$x^* = \left[i_{L_1}^*, v_{C_1}^*, i_{L_2}^*, v_{C_2}^*\right]^T \tag{6}$$

where $i_{L_1}^* = k^*$, $v_{C_1}^* = \sqrt{V_{bat}V_g}$, $i_{L_2}^* = k^*\sqrt{\frac{V_g}{V_{bat}}}$ and $v_{C_2}^* = V_o = \frac{\sqrt{V_{bat}^3} + k^*R_{bat}\sqrt{V_g}}{\sqrt{V_{bat}}}$.

Taking into account the equations (4), (5), and (6), the ideal sliding dynamics can be linearized as:

$$\frac{d\tilde{v}_{C_1}}{dt} = a_{11}\tilde{v}_{C_1} + a_{12}\tilde{i}_{L_2} + a_{13}\tilde{v}_{C_2} + b_{11}\tilde{k} + c_{11}\frac{d\tilde{k}}{dt}$$
$$\frac{d\tilde{i}_{L_2}}{dt} = a_{22}\tilde{v}_{C_1} + a_{21}\tilde{i}_{L_2} + a_{23}\tilde{v}_{C_2} + b_{21}\tilde{k} + c_{21}\frac{d\tilde{k}}{dt}$$
$$\frac{d\tilde{v}_{C_2}}{dt} = a_{33}\tilde{v}_{C_1} + a_{32}\tilde{i}_{L_2} + a_{33}\tilde{v}_{C_2} + b_{31}\tilde{k} + c_{31}\frac{d\tilde{k}}{dt} \tag{7}$$

The parameters $a_{ij}, b_{ij}, c_{ij}, (i, j \in \{1, 2, 3\})$ are defined as:

$$a_{11} = -\frac{k^*}{C_1\sqrt{V_gV_{bat}}} \quad a_{12} = -\frac{1}{C_1}\sqrt{\frac{V_{bat}}{V_g}}$$
$$a_{13} = 0$$
$$b_{11} = \frac{1}{C_1} \quad c_{11} = -\frac{L_1}{C_1}\frac{k^*}{\sqrt{V_gV_{bat}}}$$
$$a_{21} = \frac{2}{L_2}\sqrt{\frac{V_{bat}}{V_g}} \quad a_{22} = 0$$
$$a_{23} = -\frac{1}{L_2}$$
$$b_{21} = 0 \quad c_{21} = \frac{L_1}{L_2}\sqrt{\frac{V_{bat}}{V_g}}$$
$$a_{31} = 0 \quad a_{32} = \frac{1}{C_2}$$
$$a_{33} = -\frac{1}{R_{bat}C_2}$$
$$b_{31} = 0 \quad c_{31} = 0$$

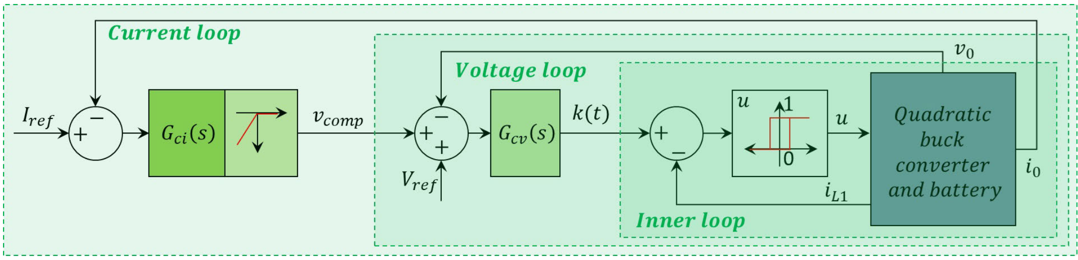

FIGURE 3. Proposed battery charger control architecture.

By applying the Laplace transform to (7), the transfer function given by (8) is obtained:

$$G_{vk}(s) = \frac{\tilde{v}_{C_2}(s)}{\tilde{k}(s)} = \frac{\beta_2 s^2 + \beta_1 s + \beta_0}{s^3 + \alpha_2 s^2 + \alpha_1 s + \alpha_0} \tag{8}$$

where

$$\beta_2 = a_{32}c_{21} \quad \beta_1 = a_{32}\left(c_{11}a_{21} - a_{11}c_{21}\right)$$
$$\beta_0 = a_{32}b_{11}a_{21} \quad \alpha_2 = -a_{11} - a_{33}$$
$$\alpha_1 = \left(a_{11}a_{33} - a_{23}a_{32} - a_{12}a_{21}\right)$$
$$\alpha_0 = \left(a_{11}a_{23}a_{32} + a_{12}a_{21}a_{33}\right)$$

IV. BATTERY CHARGING CONTROL

A. CONTROL ARCHITECTURE AND CHARGING METHOD

The control scheme depicted in Figure 3 is proposed to apply the CC-CV charging protocol. This is achieved by using an inner loop of current control based on sliding mode and two nested outer loops regulating the voltage and current of the battery. Specifically, the sliding mode controller acts on the inductor current i_{L_1} stabilizing the operation of the converter. The reference of this control loop, $k(t)$, is given by a first outer loop, which is composed of a PI compensator that acts minimizing the output voltage error. The reference of this loop is obtained as the sum of the desired voltage for the CV phase denoted as V_{ref} and the contribution of the most outer loop regulating the current of the battery and denoted as v_{comp}. Since this current is a function of the output voltage and the instantaneous static impedance of the battery, the current limitation during the CC phase can be provided by another PI compensator acting on the battery current error and tracking the reference I_{ref}. As can be observed in the scheme of Figure 3, the contribution of this last control loop is saturated at zero, thus, v_{comp} takes only negative values reducing the battery voltage during the CC phase. The PI controllers of the first and second outer loops follow the form:

$$G_{cn}(s) = \frac{K_{pn}s + K_{in}}{s} \tag{9}$$

where $n = \{v, i\}$ indicates the voltage or current loop, respectively. A detailed description of the methods used to synthesize the controllers is provided hereinafter.

B. BATTERY VOLTAGE CONTROL LOOP

In order to design the PI controller of the voltage regulation loop, the RLS-MIGO method is employed. First of all, we introduce some definitions. The loop function of the voltage regulation loop is $L(j\omega) = G_{cv}(j\omega)G_{vk}(j\omega)$, the sensitivity function is given by $S(j\omega) = \frac{1}{1+L(j\omega)}$ and the complementary sensitivity function can be expressed by $T(j\omega) = 1 - S(j\omega) = \frac{L(j\omega)}{1+L(j\omega)}$. By defining that $M_s = \sup|S(j\omega)|$ and $M_t = \sup|T(j\omega)|$, three different circular robustness regions can be obtained as listed in table 1.

TABLE 1. Centers and radius of the circular robustness regions for constant sensitivity.

Contour	Center c	Radius r
M_s	-1	$\frac{1}{M_s}$
M_t	$-\frac{M_t^2}{M_t^2-1}$	$\frac{M_t}{M_t^2-1}$
$M = M_s = M_t$	$\frac{2M^2-2M+1}{2M(M-1)}$	$\frac{2M-1}{2M(M-1)}$

The closed loop will be asymptotically stable if the Nyquist curve of the loop function $L(s)$ is outside of one the circles depending of the selected contour. While the circles defined for M_s and M_t ensure a good response to disturbances and set-point changes respectively, the use of the combined sensitivity defined by M enforces a good performance in both responses and faces the uncertainty in the converter parameters. The transfer function G_{vk} in (8) can be expressed in terms of its magnitude ($\rho(\omega)$) and phase ($\phi(\omega)$) as it is defined by expression (10).

$$G_{vk}(j\omega) = \rho(\omega)[cos(\phi(\omega)) + jsin(\phi(\omega))] \tag{10}$$

Then, the restriction to ensure the robustness is then defined as:

$$\left(K_p + \frac{cos(\phi(\omega))}{\rho(\omega)}c\right)^2 + \frac{1}{\omega^2}\left(K_i + \frac{sin(\phi(\omega))}{\rho(\omega)}\omega c\right)^2 \geq \frac{r^2}{\rho^2} \tag{11}$$

The synthesis of the voltage controller is performed by means of the following step-by-step procedure:

1) Select a value for M (generally $1.4 \leq M \leq 2$) and compute the corresponding center c and radius r of the circular robustness region.
2) Define a discrete range for ω (R_ω).

3) Define a discrete range for K_p (R_{K_p}).
4) For each value of ω ($\omega_a \in R_\omega$):
   - Compute $\rho(\omega_a)$ and $\phi(\omega_a)$.
   - Compute K_i sweeping K_p into R_{K_p} generating an ellipse in the $K_p - K_i$ plane.
5) Determine the envelope produced as the limit of the region of intersection of the ellipses.
6) Among the obtained solutions, retain the coordinate that maximizes K_i in the envelope.
7) Repeat the procedure for critical points into the set of operational conditions.
8) Among the obtained solutions, retain the coordinate with the lower K_i value.

The transfer function used for the design is $G_{vk}(s)$ (Expression (8)). Thus, the closed loop transfer function of the voltage regulation loop is obtained as follows:

$$G_{vbat}(s) = \frac{G_{vk}(s)G_{cv}(s)}{1 + G_{vk}(s)G_{cv}(s)} \tag{12}$$

C. BATTERY CURRENT CONTROL LOOP

The output voltage of the converter is applied to the battery producing a current which is dependent of the state of charge (SoC). Considering the most basic model of a battery involving a voltage source in series with a resistance, the dynamic model for the battery current can be derived as:

$$i_{bat} = \frac{v_{C_2} - v_{bat}}{R_{bat}} \tag{13}$$

Then, from (12), the transfer function used for the design is as follows:

$$G_{iv}(s) = \frac{G_{vbat}(s)}{R_{bat}} \tag{14}$$

As it s evident, the value of the battery resistance has a high influence in the loop gain which is relevant considering that this parameter is one of those that introduces greater uncertainty into the system. The closed loop transfer function of the current regulation loop is obtained as follows:

$$G_{ibat}(s) = \frac{G_{iv}(s)G_{ci}(s)}{1 + G_{iv}(s)G_{ci}(s)} \tag{15}$$

During the normal operation of the battery charger, the reference of this loop is constant and the unique disturbance is the increment in the internal voltage of the battery which is produced very slowly. This consideration allows to apply the conventional criteria for design of cascade control systems, as for example, specifying a settling time ten times higher the one of the voltage loop. By considering no overshoot in the time response, the design of this controller can be easily performed by applying the root locus method.

V. NUMERICAL RESULTS

A. SYNTHESIS OF THE VOLTAGE CONTROLLER

The assessment of the correct operation of the proposed control is performed considering a case study defined by the constrains listed in table 2.

TABLE 2. System specifications.

Symbol	Parameter	Value
P	Rated power	540 W
V_o	Output voltage	42-48 V
V_{bat}	Battery voltage	40.5-48 V
I_{bat}	Output current	10 A
V_g	Input voltage	380 V
R_{bat}	Battery resistance	100 $m\Omega$

To design the passive components of the converter, it is considered that ripples in currents do not exceed 20 % of the rated mean value of the corresponding current and ripples in voltages do not exceed 5 % of the corresponding voltage. The results are listed in table 3.

TABLE 3. Converter parameters.

Symbol	Parameter	Value
L_1	Input inductor	1.2 mH
L_2	Output inductor	0.3 mH
C_1	Input capacitor	0.3 mF
C_2	output capacitor	0.1 mF

The RLS-MIGO method presented above has been applied to synthesize the voltage controller. A value of M = 2 has been selected in the step 1. After that, a first execution of the algorithm exploring the generation of the ellipses, allows us to define the ranges $R_\omega = \{0, 10000\}$ rad/s and $R_{K_p} = \{0, 5\}$ for steps 2 and 3. Then, the algorithm produces multiple superimposed ellipses in step 4 drawing the shadowed areas in the graphics of Figure 4. These areas delineate an envelope which is the limit between the clean area and the area covered by the ellipses as defined in step 5. In each figure, the point of coordinates K_p-K_i maximizing the K_i component is indicated following the procedure defined in steps 6 and 7. The procedure is repeated for three different operation points of the charging protocol and for two different values of the internal resistance of the battery. Among the obtained options satisfying the robustness criteria for the whole operation conditions set, the gains finally selected in the step 8 of the procedure are $K_{pv} = 0$ and $K_{iv} = 454$ (Figure 4a). To verify that this selection satisfy the design criteria, Figure 5 depicts the Nyquist curves obtained for seven operation points along the charging trajectory (42 V @ 10 A, 45 V @ 10 A, 48 V @ 10 A, 48 V @ 9 A, 48 V @ 8 A, 48 V @ 7 A, 48 V @ 5 A, y 48 V @ 3 A) and for three different battery resistances (50 $m\Omega$, 100 $m\Omega$, y 150 $m\Omega$). As it can be noted, all the curves are outside of the robustness region while for higher values of the battery resistance the curves are far of the robustness region.

B. SYNTHESIS OF THE CURRENT CONTROLLER

Although the order of the resulting closed-loop dynamics of the voltage loop is four, by assessing the response to step changes in the reference for different operation points, it can be concluded that its behavior is similar to that of a first order system. This fact allows to apply the order reduction simplifying the design avoiding unnecessary complexity.

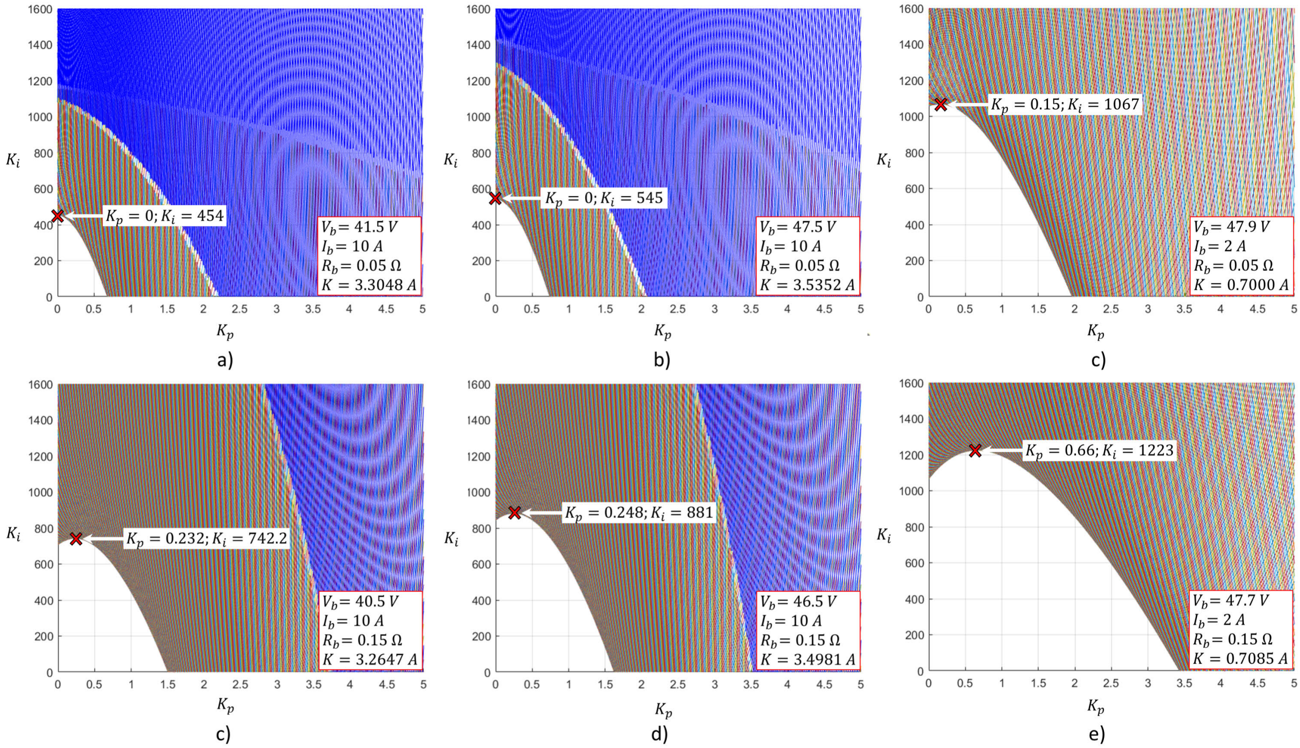

FIGURE 4. Optimization of the parameters of the voltage loop controller in the K_p-K_i plane for different operation conditions and battery model parameters.

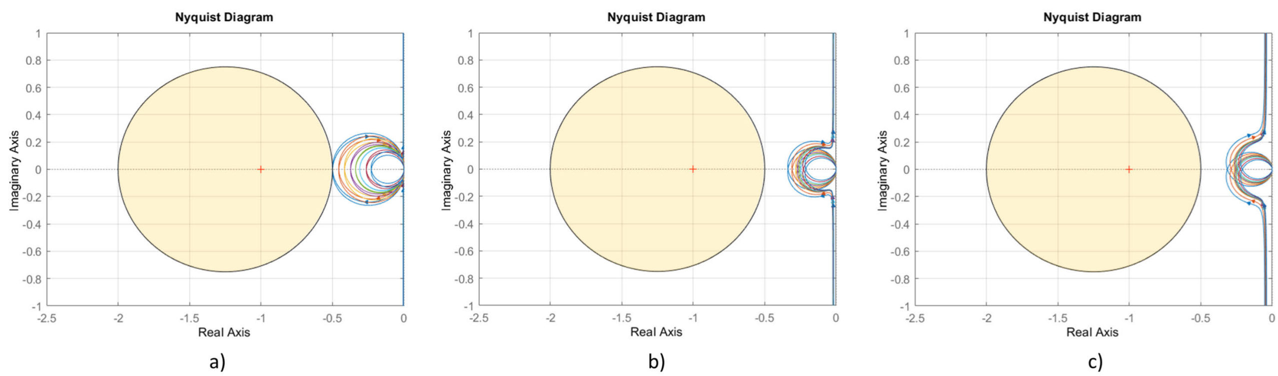

FIGURE 5. Nyquist diagram showing the robustness region and the curves for seven operation points considering different values of the battery resistance: a) 50 $m\Omega$, b) 100 $m\Omega$, and c) 150 $m\Omega$.

Figure 6 shows step responses of the closed-loop transfer function of the voltage loop for different operation conditions and for the two extreme values of the battery resistance. Also, Figure 6 shows the step response of the first order approximation that has been used for the design of the current controller whose time constant is $\tau = 9\ ms$ obtaining a settling time of around 40 ms.

Considering the above result for the voltage loop, the specifications for the current loop are a settling time of 400 ms and no overshoot. The synthesis of the controller has been assisted by the Control Systems Designer of MATLAB© by using the root locus method. The resulting gains are $K_{pi} = 0.01$ and $K_{ii} = 1.5$. Figure 7 shows step response of the closed-loop transfer function of the current loop for different points among the operation conditions and the two extreme values of the battery resistance. It is possible to observe that the settling time of the loop is obtained between 100 ms and 400 ms, which exceeds the needs of such a slow control loop. As expected, the response for values of battery resistance between the extreme values will be inside the range between the obtained limits of settling time.

C. SIMULATION RESULTS

The power converter circuit and battery models have been simulated using PSIM© software according to the circuit scheme described in Figure 1. The parameters of the converter defined in Table 3 have been used as well as a hysteresis band of ± 1 A. First simulations have been performed in

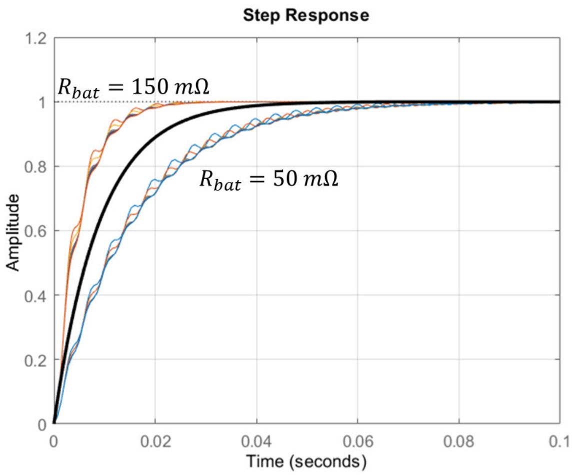

FIGURE 6. Step response of the voltage regulation loop for different operation conditions and the selected first order approximation.

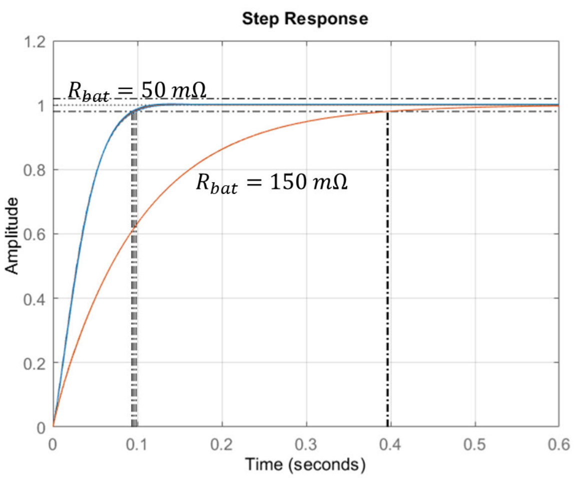

FIGURE 7. Step response of the current regulation loop for different operation conditions.

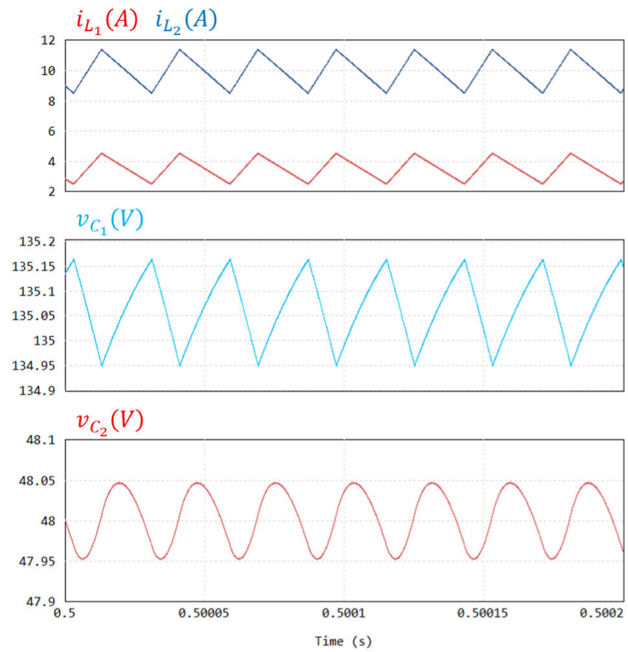

FIGURE 8. Steady-state waveforms of the converter variables when the system operates in the interface of the CC and CV phases of the charging process.

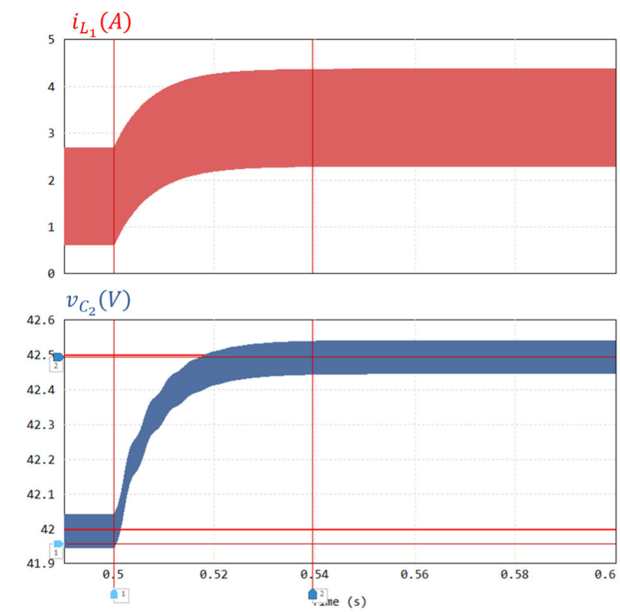

FIGURE 9. Simulated step response of the voltage regulation loop.

order to verify the stable operation of the converter along a charging cycle. Figure 8 shows the high frequency ripples for a selected steady-state of the converter variables which corresponds to the point of interface between the CC and the CV phase (48 V @ 10 A for a v_{bat} of 47 V). Also, it is possible to confirm that the mean values of the current and voltages correspond to the equilibrium defined by expression (6).

After verifying that sliding mode is adequately enforced for different conditions, the performance of the outer loops is evaluated by means of the application of step type variations in the different inputs of the system. Figure 9 shows the response of the system to a step change from 42 to 42.5 V in the voltage reference considering a constant battery voltage of 41.5 V and a null contribution of the outer current loop. It is possible to observe that the new reference is attained in a settling time of around 40 ms without overshoot as expected from the controller design specifications.

Figure 10 shows the response of the system to a step change in the current reference from 5 to 10 A considering a constant battery voltage of 42 V and a voltage reference of 48 V. Considering these constrains, the starting and the final points of the step change are in the set in which the current outer loop contribute to define the applied voltage. As it is observed, the proposed cascade control system operates as it was specified during the design process showing no overshoot and a settling time around 350 ms.

To further evaluate the performance of the proposed control system, we have applied sudden increasing and decreasing changes in the battery resistance between 50 $m\Omega$ to 150 $m\Omega$ for a constant value of the inner battery voltage of 44 V. The

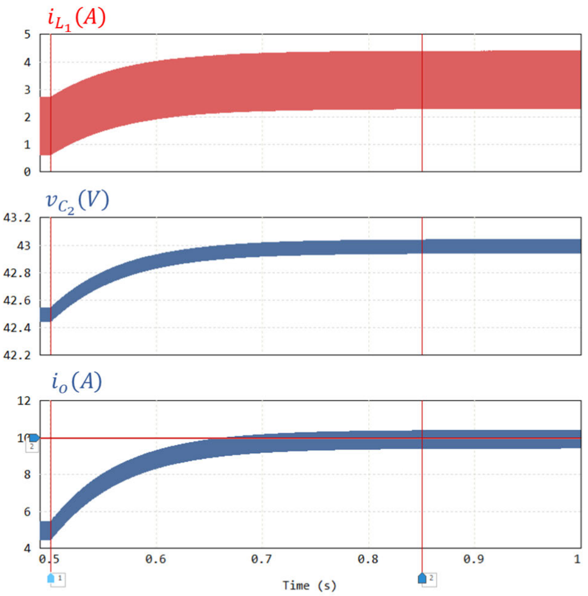

FIGURE 10. Simulated step response of the current regulation loop.

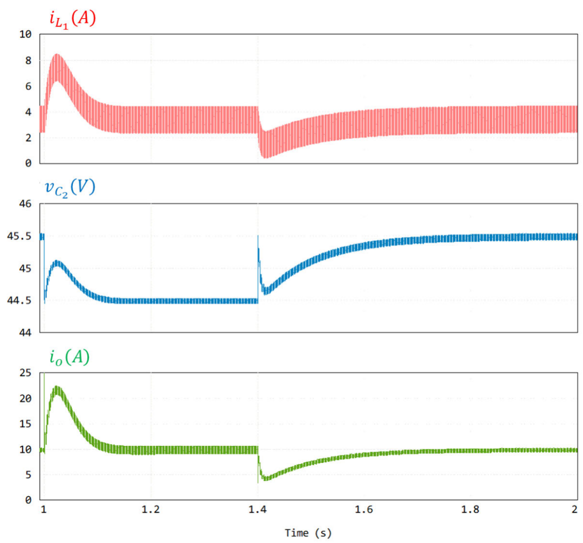

FIGURE 11. Simulated step response of the whole control system to step changes in the battery resistance within the design limits.

results are depicted in Figure 11. As it can be observed, the increasing change is rejected in less than 200 *ms* while the decreasing change is rejected in less than 400 *ms*. Although this type of change rarely occurs in the actual battery charging application, it is very challenging from the theoretical point of view to prove the robustness of the proposed control.

VI. EXPERIMENTAL RESULTS

A prototype of the proposed battery charging system composed of a power stage and a control circuit has been implemented in the laboratory. The power stage consists of two inductors (L_1, L_2) built in the laboratory, two capacitors C_1 (VISHAY 1848C MKP) and C_2 (KEMET R60 MKT), three diodes (STTH60RQ06W), and one MOSFET

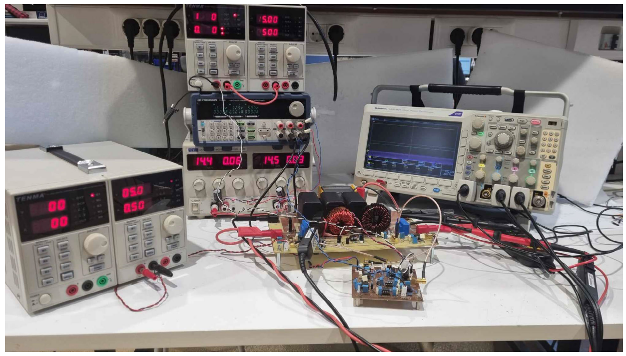

FIGURE 12. Experimental set-up and laboratory prototype.

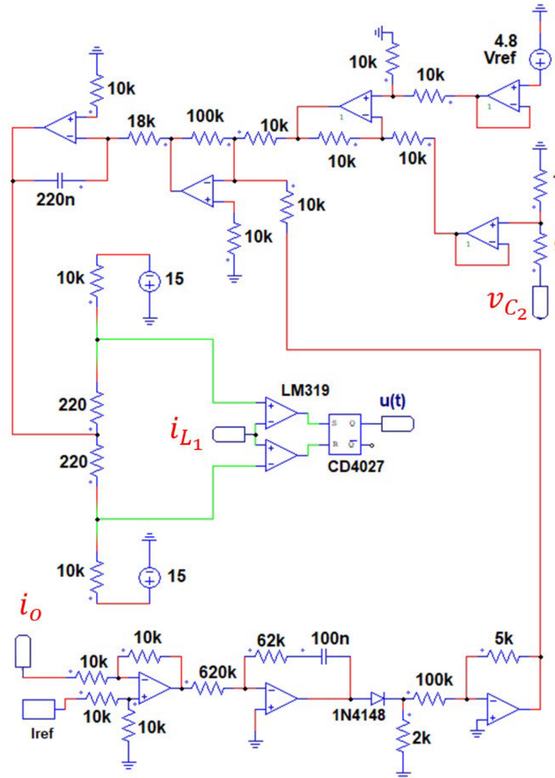

FIGURE 13. Schematic diagram of the implemented control circuit.

(IXFX52N100X). The inductor current i_{L_1} and the battery current i_o are measured using Hall-effect current sensors (LAH25-NP) with gains 0.6 and 0.2 respectively, while the output voltage is sensed using a differential operational amplifier (AD629ANZ) having a gain of 0.1. A power supply SPS 800 $\times$ 13 is used as input voltage source for the QBC (380 V). The references for the voltage and current loops have been provided by an external precision voltage source. The experimental results have been taken by an oscilloscope TEKTRONIX (MDO3024) using a differential voltage probe (THDP0200) for measuring the output voltage and two current probes (TCP0020) for measuring the battery current and the inductor current i_{L_1}. The photography of the experimental set-up and the prototype is depicted in Figure 12.

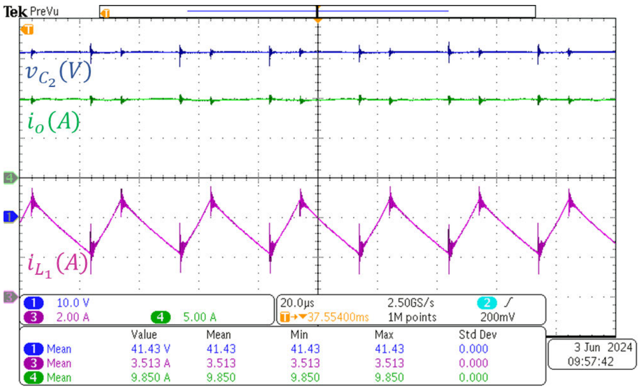

(a) CC phase.

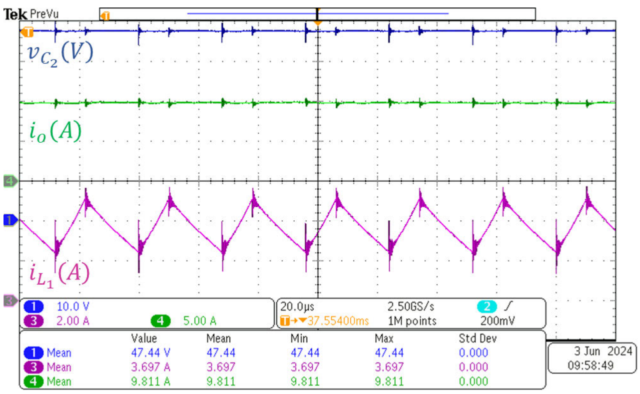

(b) Interface between CC and CV phases.

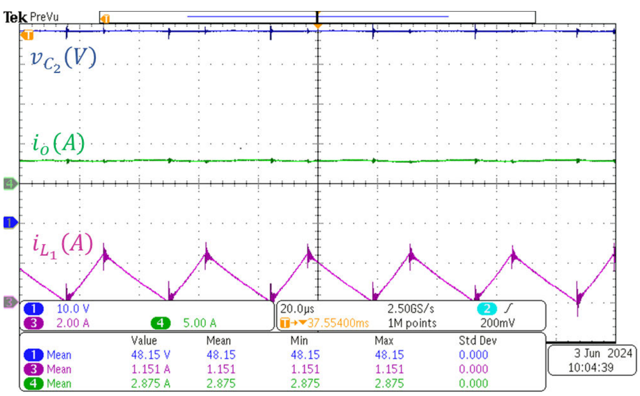

(c) CV phase.

FIGURE 14. Experimental waveforms of the steady-state of the converter variables.

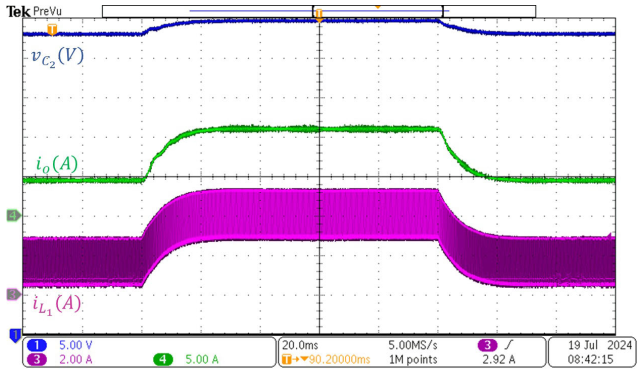

FIGURE 15. Experimental step response of the voltage regulation loop.

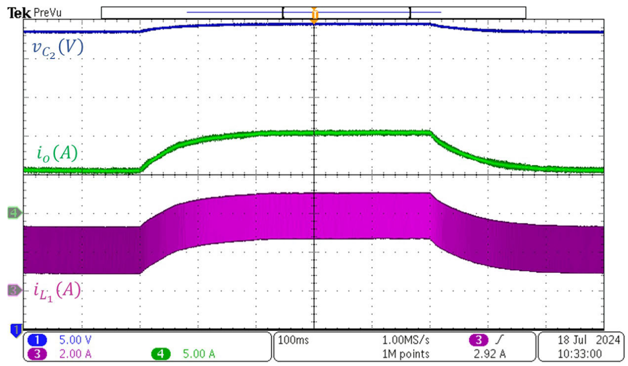

FIGURE 16. Experimental step response of the current regulation loop.

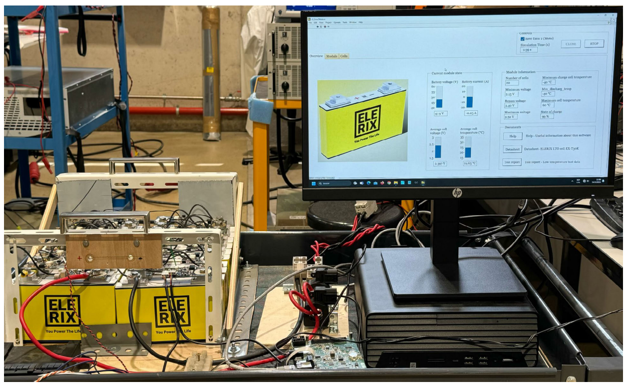

FIGURE 17. Battery array and SCADA system for data acquisition.

The sliding mode control loop has been implemented by means of an hysteresis comparator composed of one flip-flop (CD4027BE) and two comparators (LM319N). Equally than in the simulation model, the hysteresis band has been defined as ± 1 A limiting the maximum switching frequency below 80 kHz. The linear controllers and mathematical operations have been implemented using standard operational amplifiers (MC33078P). The complete scheme of the control circuit is illustrated in Figure 13.

To test the system, the first step consists in obtaining the converter waveforms in key operation points of the charging process. An electronic load REGATRON G5.RSS has been used working as a battery, with inner voltage varying between 42 and 48 V and an internal resistance of 100 $m\Omega$. Figure 14 shows the oscilloscope capture of the inductor current, the output voltage and the output current for one point at the start of the charging process during the constant-current phase (42 V @ 10 A), one point in the interface between the CC phase and the CV phase (48 V @ 10 A), and one point during the CV phase (48 V, 2 A).

After verifying that sliding mode is adequately enforced in the inner current control loop, the performance of the voltage and current loops is evaluated by applying step type variations in their references. Figure 15 shows the response

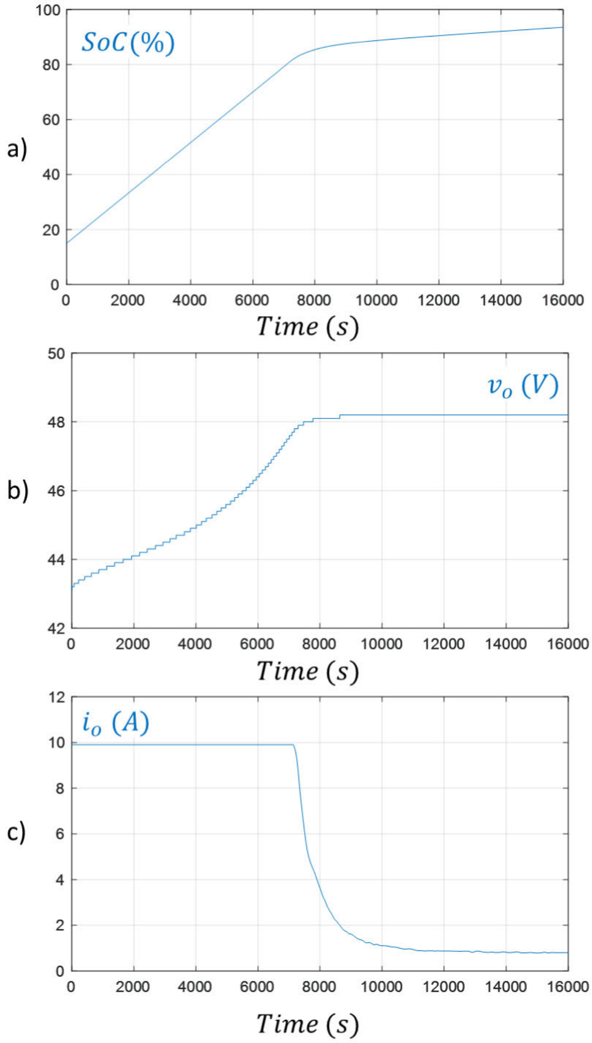

FIGURE 18. Experimental results for one cycle of the CC-CV charging protocol: a) SoC, b) battery voltage, and c) battery current.

of the system to a step change in the voltage reference from 42 to 42.5 V considering a constant battery voltage of 41.5 V and disconnecting the outer current loop. It is possible to observe that the new reference is attained in a settling time of around 40 ms as expected from the simulation results. Figure 16 shows the response of the current loop to a step change in the reference from 5 to 10 A considering a constant battery voltage of 42 V and a reference of 48 V for the voltage loop. It is possible to observe that the new reference is attained in a settling time of around 350 ms as expected from simulations.

After verifying the correct operation of the system under controlled conditions, a test using real batteries (20 cells of 30 Ah - ELERIX Lithium Titanate Oxide) has been developed. Figure 17 shows a photography of the battery array used in the experiments and the acquisition system developed in LabVIEW© to obtain the data. Figure 18 shows the experimental results obtained from a complete cycle of charge of the battery where the CC and CV phases can be clearly differentiated. The figure depicts the current and voltage measurements and the SoC computation, the latter having been obtained by means of the ampere hour counting method. The complete charging process at 0.33C rate takes place in 16.000 s approximately, of which almost half of the time corresponds to the CC phase and the rest to the CV phase. The estimated initial SoC is 15%.

VII. CONCLUSION

In this paper, the quadratic buck converter has been studied as a suitable alternative for battery charging by obtaining a high step-up current gain without the use of bulky transformers. Besides, due to the higher-order of the QBC, a control based on a SMC has been applied to achieve robustness and faster response with respect to a linear control approach. As a result, a multi-loop controller using three nested loops has been implemented involving one sliding mode current controller and two conventional PI controllers. The selected sliding surface uses only the inductor current nearest to the input port because the selection of any of the other variables leads to an unstable behavior and the linear combination of more than one variable adds complexity but does not improve the performance of the inductor current control. Finally, the robustness of the whole system has been introduced by means of the RLS-MIGO method ensuring the better performance of the PI controller regulating the output voltage. In addition, the PI controller regulating the output current has been designed following conventional rules of cascade controllers. Simulated and experimental results show that the quadratic buck converter operates properly following the conventional CC-CV charging protocol by using the proposed control scheme. Future work contemplates the association of QBCs in paralleling [40] or in interleaving [41] to obtain battery ultrafast charging, and comparison in terms of efficiency of the quadratic buck topology with the cascade connection of two buck stages sharing the same control signal both operating in sliding-mode.

REFERENCES

[1] S. Stynski, W. Luo, A. Chub, L. G. Franquelo, M. Malinowski, and D. Vinnikov, "Utility-scale energy storage systems: Converters and control," *IEEE Ind. Electron. Mag.*, vol. 14, no. 4, pp. 32–52, Dec. 2020.

[2] W. Luo, S. Stynski, A. Chub, L. G. Franquelo, M. Malinowski, and D. Vinnikov, "Utility-scale energy storage systems: A comprehensive review of their applications, challenges, and future directions," *IEEE Ind. Electron. Mag.*, vol. 15, no. 4, pp. 17–27, Dec. 2021.

[3] J. Cao and A. Emadi, "Batteries need electronics," *IEEE Ind. Electron. Mag.*, vol. 5, no. 1, pp. 27–35, Mar. 2011.

[4] K. L. Pham, J. Leuchter, R. Bystricky, M. Andrle, N. N. Pham, and V. T. Pham, "The study of electrical energy power supply system for UAVs based on the energy storage technology," *Aerospace*, vol. 9, no. 9, p. 500, Sep. 2022.

[5] S. Rivera, S. M. Goetz, S. Kouro, P. W. Lehn, M. Pathmanathan, P. Bauer, and R. A. Mastromauro, "Charging infrastructure and grid integration for electromobility," *Proc. IEEE*, vol. 111, no. 4, pp. 371–396, Apr. 2023.

[6] S. Rivera, S. Kouro, S. Vazquez, S. M. Goetz, R. Lizana, and E. Romero-Cadaval, "Electric vehicle charging infrastructure: From grid to battery," *IEEE Ind. Electron. Mag.*, vol. 15, no. 2, pp. 37–51, Jun. 2021.

[7] A. Elezab, O. Zayed, A. Abuelnaga, and M. Narimani, "High efficiency LLC resonant converter with wide output range of 200–1000 V for DC-connected EVs ultra-fast charging stations," *IEEE Access*, vol. 11, pp. 33037–33048, 2023.

[8] D. Zambrano-Prada, A. Blanch-Fortuna, J. A. Barrado-Rodrigo, L. Vázquez-Seisdedos, O. López-Santos, A. E. Aroudi, and L. Martinez-Salamero, ''Electrical architecture for ultrafast charging station,'' *Transp. Res. Proc.*, vol. 70, pp. 170–177, Jan. 2023.

[9] M. Safayatullah, M. T. Elrais, S. Ghosh, R. Rezaii, and I. Batarseh, ''A comprehensive review of power converter topologies and control methods for electric vehicle fast charging applications,'' *IEEE Access*, vol. 10, pp. 40753–40793, 2022.

[10] C. Wang, T. Liu, X. Tang, S. Ge, N. Stanley, E. Rountree, Y. Leng, and B. McCarthy, ''Fast charging of energy-dense lithium-ion batteries,'' *Nature*, vol. 611, pp. 485–490, Oct. 2022.

[11] C. Chen, Z. Wei, and A. C. Knoll, ''Charging optimization for Li-ion battery in electric vehicles: A review,'' *IEEE Trans. Transport. Electrific.*, vol. 8, no. 3, pp. 3068–3089, Sep. 2022.

[12] G.-J. Chen and W.-H. Chung, ''Evaluation of charging methods for lithium-ion batteries,'' *Electronics*, vol. 12, no. 19, p. 4095, Sep. 2023.

[13] B.-Y. Chen and Y.-S. Lai, ''New digital-controlled technique for battery charger with constant current and voltage control without current feedback,'' *IEEE Trans. Ind. Electron.*, vol. 59, no. 3, pp. 1545–1553, Mar. 2012.

[14] J. Deng, S. Li, S. Hu, C. C. Mi, and R. Ma, ''Design methodology of LLC resonant converters for electric vehicle battery chargers,'' *IEEE Trans. Veh. Technol.*, vol. 63, no. 4, pp. 1581–1592, May 2014.

[15] D. Lyu, T. B. Soeiro, and P. Bauer, ''Impacts of different charging strategies on the electric vehicle battery charger circuit using phase-shift full-bridge converter,'' in *Proc. IEEE 19th Int. Power Electron. Motion Control Conf. (PEMC)*, Apr. 2021, pp. 256–263.

[16] O. Lopez-Santos, D. Zambrano-Prada, L. Martinez-Salamero, A. E. Aroudi, and L. Vazquez-Seisdedos, ''Unidirectional DC–DC converters for ultrafast charging of electric vehicles,'' in *Proc. IEEE Int. Conf. Electr. Syst. Aircr., Railway, Ship Propuls. Road Vehicles Int. Transp. Electrific. Conf. (ESARS-ITEC)*, Mar. 2023, pp. 1–6.

[17] D. Maksimovic and S. Cuk, ''Switching converters with wide DC conversion range,'' *IEEE Trans. Power Electron.*, vol. 6, no. 1, pp. 151–157, Jan. 1991.

[18] E. Carbajal-Gutierrez, J. Morales-Saldana, and J. Leyva-Ramos, ''Modeling of a single-switch quadratic buck converter,'' *IEEE Trans. Aerosp. Electron. Syst.*, vol. 41, no. 4, pp. 1450–1456, Oct. 2005.

[19] J. A. Morales-Saldana, J. Leyva-Ramos, E. E. Carbajal-Gutierrez, and M. G. Ortiz-Lopez, ''Average current-mode control scheme for a quadratic buck converter with a single switch,'' *IEEE Trans. Power Electron.*, vol. 23, no. 1, pp. 485–490, Jan. 2008.

[20] I. A. Reyes-Portillo, J. A. Morales-Saldaña, E. M. Netzahuatl-Huerta, E. R. Palacios-Hernández, and S. R. Méndez-Elizondo, ''Modeling of a quadratic buck converter based on the R2P2 concept for PV applications,'' in *Proc. IEEE Int. Autumn Meeting Power, Electron. Comput. (ROPEC)*, vol. 4, Nov. 2020, pp. 1–6.

[21] C. A. Torres-Pinzón, F. Flores-Bahamonde, J. A. Garriga-Castillo, H. Valderrama-Blavi, R. Haroun, and L. Martínez-Salamero, ''Sliding-mode control of a quadratic buck converter with constant power load,'' *IEEE Access*, vol. 10, pp. 71837–71852, 2022.

[22] X. Zhang, T. Wang, H. Bao, Y. Hu, and B. Bao, ''Stability effect of load converter on source converter in a cascaded buck converter,'' *IEEE Trans. Power Electron.*, vol. 38, no. 1, pp. 604–618, Jan. 2023.

[23] S.-C. Tan, Y. M. Lai, and C. K. Tse, ''General design issues of sliding-mode controllers in DC–DC converters,'' *IEEE Trans. Ind. Electron.*, vol. 55, no. 3, pp. 1160–1174, Mar. 2008.

[24] L. Martinez-Salamero, A. Cid-Pastor, A. ElAroudi, R. Giral, J. Calvente, and G. Ruiz-Magaz, ''Sliding-mode control of DC–DC switching converters,'' in *Proc. IFAC World Conf.*, Milano, Italy, 2011, vol. 44, no. 1, pp. 1910–1916.

[25] D. A. Zambrano-Prada, A. El Aroudi, L. Vázquez-Seisdedos, and L. Martínez-Salamero, ''Polynomial sliding surfaces to control a boost converter with constant power load,'' *IEEE Trans. Circuits Syst. I, Reg. Papers*, vol. 70, no. 1, pp. 530–543, Jan. 2023.

[26] E. Vidal-Idiarte, C. E. Carrejo, J. Calvente, and L. Martínez-Salamero, ''Two-loop digital sliding mode control of DC–DC power converters based on predictive interpolation,'' *IEEE Trans. Ind. Electron.*, vol. 58, no. 6, pp. 2491–2501, Jun. 2011.

[27] O. Lopez-Santos, G. Garcia, L. Martinez-Salamero, J. C. Avila-Martinez, and L. Seguier, ''Non-linear control of the output stage of a solar microinverter,'' *Int. J. Control*, vol. 90, no. 1, pp. 90–109, Jan. 2017.

[28] F. Flores-Bahamonde, H. Valderrama-Blavi, J. M. Bosque-Moncusi, G. García, and L. Martínez-Salamero, ''Using the sliding-mode control approach for analysis and design of the boost inverter,'' *IET Power Electron.*, vol. 9, no. 8, pp. 1625–1634, Jun. 2016.

[29] O. López-Santos and G. García, ''Double sliding-surface multiloop control reducing semiconductor voltage stress on the boost inverter,'' *Appl. Sci.*, vol. 10, no. 14, p. 4912, Jul. 2020.

[30] O. Lopez-Santos, L. Martinez-Salamero, G. Garcia, H. Valderrama-Blavi, and T. Sierra-Polanco, ''Robust sliding-mode control design for a voltage regulated quadratic boost converter,'' *IEEE Trans. Power Electron.*, vol. 30, no. 4, pp. 2313–2327, Apr. 2015.

[31] Z. Chen, ''PI and sliding mode control of a Cuk converter,'' *IEEE Trans. Power Electron.*, vol. 27, no. 8, pp. 3695–3703, Aug. 2012.

[32] O. Lopez-Santos, D. Z. Prada, Y. Aldana-Rodriguez, H. Esquivel-Cabeza, G. Garcia, and L. Martinez-Salamero, ''Control of a bidirectional cuk converter providing charge/discharge of a battery array integrated in DC buses of microgrids,'' in *Proc. Workshop Eng. Appl.*, vol. 742, Aug. 2017, pp. 495–507.

[33] H. Panagopoulos and K. Astrom, ''PID control design and H_∞ loop shaping,'' *Int. J. Robust Nonlinear Control*, vol. 10, no. 15, pp. 1249–1261, Dec. 2000.

[34] H. Panagopoulos, T. Hägglund, and K. J. Åström, ''Design of PID controllers based on constrained optimisation,'' *IEE Proc. - Control Theory Appl.*, vol. 149, no. 1, pp. 32–40, Jan. 2002.

[35] K. J. Åström, H. Panagopoulos, and T. Hägglund, ''Design of PI controllers based on non-convex optimization,'' *Automatica*, vol. 34, no. 5, pp. 585–601, May 1998.

[36] O. Lopez-Santos, A. Barbosa-Escobar, and G. Garcia, ''A robust multi-loop linear controller for transformer-based single-phase PWM inverter,'' in *Proc. IEEE Workshop Power Electron. Power Quality Appl. (PEPQA)*, May 2017, pp. 1–8.

[37] K. S. Reddy, R. Jeyasenthil, and T. Kobaku, ''QFT approach to robust control of DC–DC buck converter,'' in *Proc. IEEE Int. Conf. Power Electron., Drives Energy Syst. (PEDES)*, Dec. 2022, pp. 1–6.

[38] R. Sharma, A. Maulik, and S. Kamal, ''Robust control of an islanded DC microgrid using H_∞ loop-shaping design considering parametric uncertainties,'' in *Proc. TENCON IEEE Region Conf. (TENCON)*, Oct. 2023, pp. 1–6.

[39] O. López-Santos, F. Flores-Bahamonde, C. A. Torres-Pinzón, R. Haroun, H. Valderrama-Blavi, J. A. Garriga, and L. Martínez-Salamero, ''Multi-loop sliding-mode control for a battery charger using a quadratic buck converter,'' in *Proc. IEEE 8th Southern Power Electron. Conf. 17th Brazilian Power Electron. Conf. (SPEC/COBEP)*, Nov. 2023, pp. 1–5.

[40] A. Cid-Pastor, L. Martinez-Salamero, C. Alonso, R. Leyva, and S. Singer, ''Paralleling DC–DC switching converters by means of power gyrators,'' *IEEE Trans. Power Electron.*, vol. 22, no. 6, pp. 2444–2453, Nov. 2007.

[41] S. Ozeri, D. Shmilovitz, S. Singer, and L. Martinez-Salamero, ''The mathematical foundation of distributed interleaved systems,'' *IEEE Trans. Circuits Syst. I, Reg. Papers*, vol. 54, no. 3, pp. 610–619, Mar. 2007.

OSWALDO LÓPEZ-SANTOS (Senior Member, IEEE) received the bachelor's degree in electronics engineering from Universidad Distrital Francisco José de Caldas, Bogotá, Colombia, in 2002, the master's degree in industrial automation from Universidad Nacional de Colombia, Bogotá, in 2011, and the Ph.D. degree from the Institut National des Sciences Appliquées (INSA) de Toulouse, in 2015. He developing his research project at LAAS-CNRS. From 2004 to 2008, he worked in Colombia as a Design Engineer for the manufacture of industrial power converters. From 2009 to 2021, he was an Associate Professor with the Department of Electronics Engineering and the Leader of the Research Group D+Tec (Technological Development), Universidad de Ibagué, Colombia, where he was the Director of the Research Office, in 2020. Currently, he is a Researcher with the Research Group GAEI, Universitat Rovira i Virgili, Tarragona, Spain. His current research interests include the control of power electronic converters involved in applications, such as microgrids and electric vehicles.

CARLOS ANDRÉS TORRES-PINZÓN received the bachelor's and master's degrees in electrical engineering from Universidad Tecnológica de Pereira (UTP), Pereira, Colombia, in 2006 and 2008, respectively, and the master's and Ph.D. degrees in electronic engineering from Universitat Rovira i Virgili, Tarragona, Spain, in 2010 and 2012, respectively. From 2006 to 2007, he was a Lecturer Assistant with UTP. From 2013 to 2023, he was an Associate Professor with the Faculty of Electronics Engineering and the Leader of the Modeling, Electronics and Monitoring (MEM) Research Group, Universidad Santo Tomás, Bogotá, Colombia, where he is currently the Dean of the School of Electrical Engineering. His main research interests include robust control, sliding-mode control, dc–dc converters designs, and control and energy management systems.

FREDDY FLORES-BAHAMONDE (Senior Member, IEEE) was born in Osorno, Chile, in 1983. He received the M.Sc. and Ph.D. degrees in electronics engineering from Universitat Rovira i Virgili (URV), Tarragona, Spain, in 2009 and 2013, respectively. In 2015, he joined the Advanced Center for Electrical and Electronic Engineering (AC3E), Universidad Técnica Federico Santa María (UTFSM), Valparaíso, Chile, as a Postdoctoral Fellow. In 2017, he was In-Charge of the energy area in the technology transfer unit with the AC3E developing and managing industrial projects related to energy and electric power systems. He is currently an Associate Professor with the Department of Engineering Sciences, Universidad Andrés Bello, where he is also the Director of the Energy Transformation Center. His main interests include the design and control of power converters for renewable energies, automotive power systems, and dc microgrids.

REHAM HAROUN (Member, IEEE) was born in Egypt, in 1982. She received the graduate degree in power and electrical engineering from Aswan Faculty of Engineering, South Valley University, Aswan, Egypt, in 2004, the master's degree from South Valley University, in 2009, and the Ph.D. degree from Universitat Rovira i Virgili (URV), Tarragona, Spain, in 2014. From 2004 to 2009, she was a Lecturer Assistant with South Valley University. From 2004 to 2009, she was also a member of Aswan Power Electronics Application Research Center (APEARC) Group. She is currently a Researcher with the Group of Automatic Control and Industrial Electronics (GAEI), URV. Her research interests include power electronics applications, including dc–dc switched power supplies and ac–dc converters with power factor correction (PFC).

JUAN ANTONIO GARRIGA (Member, IEEE) received the B.Sc. degree (Ingeniero Técnico) in telecommunications engineering from the Polytechnic University of Catalonia (UPC), in 1989, the Engineering degree (Ingeniero en Electronica) from the University of Barcelona (UB), in 2005, and the MSc. degree in electronic engineering and the Ph.D. degree from the University Rovira i Virgili (URV), in 2013 and 2020, respectively. He is currently a member of the Robotics and Signal Processing research Group, University of Lleida (UdL). His research interests include the design and control of dc–dc converters for energy harvesting applications.

HUGO VALDERRAMA-BLAVI (Member, IEEE) received the Graduate and Ph.D. degrees in ingeniero de telecomunicación from the Polytechnic University of Catalonia Barcelona, Spain, in 1994 and 2001, respectively. From 2001 to 2002, he was a Postdoctoral Researcher with the LAAS-CNRS, Toulouse, France, working in multilevel conversion and renewable energy systems. Since 1997, he has been with the Departament d'Enginyeria Electrónica, Elèctrica i Automàtica, Escola Tècnica Superior d'Enginyeria, Universitat Rovira i Virgili (URV), Tarragona, Spain, where he is currently an Associate Professor. Since 2018, he has directed the Master's Degree Program of URV in electric vehicle technologies. He has conducted several research projects sponsored by Spanish Ministry of Science and Innovation, and he has co-authored more than 30 journal articles and many conference papers. He is a member of the Group of Automatic Control and Industrial Electronics (GAEI), URV. His current research interests include power electronics, power conditioning for electric vehicles, microgrids, multilevel inverters, electric vehicle battery modeling, battery fast charging systems, photovoltaics systems, and other renewable energy sources.

LUIS MARTÍNEZ-SALAMERO (Life Senior Member, IEEE) received the Ingeniero de Telecomunicación and Ph.D. degrees from Universidad Politécnica de Cataluña, Barcelona, Spain, in 1978 and 1984, respectively. From 1978 to 1992, he taught circuit theory, analog electronics, and power processing with the Escuela Técnica Superior de Ingenieros de Telecomunicación, Barcelona. From 1992 to 1993, he was a Visiting Professor with the Center for Solid State Power Conditioning and Control, Department of Electrical Engineering, Duke University, Durham, NC, USA. From 2003 to 2004, from 2010 to 2011, and from March 2018 to September 2018 he was a Visiting Scholar with the Laboratory of Architecture and Systems Analysis (LAAS), National Agency for Scientific Research (CNRS), Toulouse, France. Since 1995, he has been a Full Professor with the Department of Electrical Electronic and Automatic Control Engineering, School of Electrical and Computer Engineering, Universitat Rovira i Virgili, Tarragona, Spain, where he managed the Research Group in Automatic Control and Industrial Electronics (GAEI), from 1998 to 2018. His research interests include structure and control of power conditioning systems, namely, electrical architecture of satellites and electric vehicles, as well as nonlinear control of converters and drives, and power conditioning for renewable energy.